Spectral properties of a V-type three-level atom driven by two bichromatic fields

Li, P; Nakajima, T; Ning, XJ

PHYSICAL REVIEW A **74**, 043408 (2006)

Spectral properties of a *V*-type three-level atom driven by two bichromatic fields

Peng Li,[1,2] Takashi Nakajima,[2] and Xi-Jing Ning[1,*]
[1]*Applied Ion-beam Laboratory, Institute of Modern Physics, Fudan University, Shanghai 200433, People's Republic of China*
[2]*Institute of Advanced Energy, Kyoto University, Gokasho, Uji, Kyoto 611-0011, Japan*
(Received 26 June 2006; published 12 October 2006)

We theoretically investigate the spectral properties of a *V*-type three-level atom driven by two bichromatic fields with a common frequency difference. By decomposing the master equation using harmonic expansions and invoking quantum regression theorem, fluorescence and probe absorption spectra of the strong atomic transition are numerically calculated under the steady state condition. We find that both fluorescence and absorption spectra exhibit two interesting features, which are equidistant comblike structures and phase-dependent line splittings. In the comblike structures, each fluorescence peak can be made subnatural by manipulating the relative intensities of the coupling fields, while for the absorption lines only the central peak can be narrowed. Line splittings are induced by the relative phase delay between the envelopes of the amplitudes of the two bichromatic fields. Interestingly, we find that the manipulation of the relative phase delay results in the emergence of sharp subnatural dips in the absorption spectra. As a natural consequence of the subnatural absorption dips, absorption spectra in atomic vapors exhibit striking *subnatural burning holes* for the counterpropagating probe beam geometry.

DOI: 10.1103/PhysRevA.74.043408 PACS number(s): 42.50.Hz, 32.80.Qk

I. INTRODUCTION

In the absence of an external radiation field it has been well understood that the interaction between an excited atom and the vacuum field results in the atomic spontaneous emission with an intrinsic Lorenzian line-shape termed natural width. When an atom is exposed to external radiation fields, in particular, intense laser fields, lots of things can happen, and as a result, an atomic line shape may be dramatically modified in one way or another. Depending on which interaction is much stronger compared to the others, a prediagonalization procedure of the total (laser plus atom) system under consideration may be useful to understand the dynamics, which is the primary reason of introducing the concept of *dressed states* compared with *bare states*. Thus, understanding the spectral properties of an atom interacting with intense external laser fields is one of the key problems in quantum optics.

Early studies [1] had shown that, for a two-level atom (TLA) interacting with a strong monochromatic driving field, the fluorescence spectrum exhibits the "Mollow's triplet," which consists of a central peak located at the laser field frequency and two side peaks symmetrically shifted from the central peak by the Rabi frequency of the driving field. The side peaks are one and a half times in width and one-third in height of the central peak under the secular approximation and the relative widths and heights are independent of the intensity of the laser field. If a weak probe field is further introduced, the absorption spectrum shows two dispersive line shapes symmetrically shifted from the driving field frequency by the Rabi frequency, and the probe field within the frequency range of the two Rabi sidebands may experience pronounced amplification without atomic population inversion, at the expense of attenuation of the driving field.

If the monochromatic driving field is replaced by the bichromatic driving field, spectral properties of the TLA turn out to be quite different from the Mollow's monochromatic case [2]. In particular, for the bichromatic driving field with frequency separation 2δ and equal intensity distribution between the two frequency components, if the resonant condition is satisfied in that the average of the two frequency components equals the atomic transition frequency, the fluorescence spectrum shows multiple equidistant (with spacing δ) side peaks symmetrically located with respect to the atomic transition frequency. The widths and relative intensities of the side peaks depend quantitatively on the parameter Ω/δ, which is the ratio between the Rabi frequency and the frequency separation of the bichromatic field. Moreover, widths of all side peaks located at odd multiples of δ approach one and a half times of the natural width and those for all even side peaks approach the natural width under the strong field approximation ($\Omega/\delta \gg 1$). The probe absorption spectrum appears with a similar equidistant structure but with dispersive line shapes located at each multiple of δ.

By going beyond the TLA, even more interesting spectral properties have been found for a *multilevel atom* driven by more than one external field. In this case line narrowing (subnatural linewidth) induced by quantum interference is one of the most significant outcomes, since it can be achieved without modifying the property of the vacuum field. Narducci *et al.* [3] have proved that, for a *V*-type three-level atom resonantly coupled by two monochromatic fields, Mollow's triplet can be narrowed well below the natural width, provided that the Rabi frequency corresponding to the weak atomic transition is made larger than that to the strong atomic transition. However, line narrowing in the absorption spectra cannot be realized within this model, which is consistent with the experimental findings [2,3].

Knowing the above, a natural question would be, what would happen if the Narducci's model is extended for a more

*Corresponding author. E-mail address: xjning@fudan.edu.cn

general case, through the replacement of two monochromatic fields by two bichromatic fields. Now there are three questions we would like to address: The first one is whether and how much line narrowing in the fluorescence spectrum takes place. The second one is whether and how much line narrowing of the probe absorption can be achieved. The third one is whether and how much the relative phase of the multiple bichromatic driving fields affect the fluorescence and absorption spectra. Note that the third question is relevant in this study because the two bichromatic fields can be alternatively considered as two amplitude-modulated fields, with each field modulated as $\cos(\delta t+\varphi_1)$ and $\cos(\delta t+\varphi_2)$, respectively, and therefore the relative phase delay $\Phi=\varphi_2-\varphi_1$ between these two modulating signals (usually in the radio frequency range), or equivalently the phase delay between the envelopes of the amplitudes of the two fields undoubtedly may serve as a new doorknob to manipulate the spectral properties. This is particularly interesting when we recall the fact that the phase dependence has not been found for the TLA driven by a single bichromatic field [2,4,5].

The purpose of this paper is to theoretically study the spectral properties of a *V*-type three-level atom driven by *two* bichromatic fields with a common frequency spacing of 2δ for each bichromatic field. After formulating the problem in terms of a master equation, we make a decomposition of the master equation using a harmonic expansion method. By further applying the quantum regression theorem, we obtain numerical solutions of the steady state spectrum for the fluorescence and the probe absorption. We find that the phase delay Φ plays a key role in manipulating the spectral shape, as expected. Numerical results show striking spectral features as below due to quantum interference: (1) Under the in-phase condition $\Phi=0$, we observe subnatural comblike fluorescence peaks which is quite similar to the line-narrowing property of the *V*-type atom driven by monochromatic fields; (2) Under the out-of-phase condition $\Phi\neq 0$, both fluorescence and absorption line shapes exhibit pronounced splittings and moreover, with small but nonzero Φ, we observe deep subnatural dips on top of the absorption peaks; (3) If the Doppler-broadening is taken into account, we find that absorption in atomic vapors exhibits significant subnatural "*burning holes*" for the counterpropagating probe beam, which is connected to the subnatural absorption dips stated in (2).

Related to our findings, subnatural narrowing of the absorption line in a Rb vapor has been experimentally studied by Rapol *et al.* [6] for a Λ-type three-level system, in which the detuned coupling field produces Autler-Towns (AT) doublet with unequal widths. One of the doublet peaks can thus be made subnatural by carefully choosing the parameters. A drawback of their scheme is the intrinsic mismatch of the subnatural line with the atomic transition frequency. Goren *et al.* [7] proposed a tripod system in which the absorption line of the circularly polarized probe field can be made both sub-Doppler and subnatural using the linearly polarized coupling field with the aid of an external static magnetic field. In a bichromatically driven Ξ-system Jakob and G. Y. Kryuchkyan [8] found that the odd multiples of AT lines are subnatural due to the mixing of two atomic decay channels induced by bichromatic field. The main difference between our work and Refs. [6,7] is the use of two bichromatic fields instead of monochromatic fields, which brings a significant phase sensitivity in the spectra. Note that very little work has been reported on the interaction of an atom with *two* bichromatic fields, except Refs. [9,10] where the main focus was on the subharmonic resonance and population trapping.

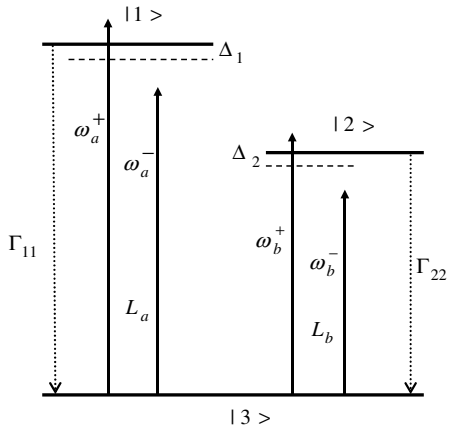

FIG. 1. A *V*-type three-level atom with excited states, $|1\rangle$ and $|2\rangle$, coupled to the common ground state, $|3\rangle$, by the two bichromatic fields L_a and L_b, respectively. Frequency components of each bichromatic field are denoted by $\omega_a^{\pm}(=\omega_a\pm\delta)$ and $\omega_b^{\pm}(=\omega_b\pm\delta)$, respectively. Spontaneous decay rate of 1–3 and 2–3 transition are denoted by Γ_{11}, and Γ_{22}, respectively.

II. THEORY

A. Model

The model we consider in this paper is depicted in Fig. 1. A *V*-type three-level atom is interacting with two bichromatic fields, L_a and L_b, each of which consists of frequency components $\omega_a\pm\delta$ and $\omega_b\pm\delta$, respectively. Therefore the fields can be written in a uniformed expression $\tilde{E}_{a,b}^{\pm}\exp[i(\omega_{a,b}\pm\delta)t]+\text{c.c.}$, where $\tilde{E}_{a,b}^{\pm}$ stand for the complex amplitude for each frequency component. We assume that the two excited states are well separated in energy so that each atomic transition is only coupled by one of the bichromatic fields.

Under the rotating-wave approximation, the interaction Hamiltonian can be written as

$$H = \hbar\begin{bmatrix} \Delta_1 & 0 & \Omega_1^+e^{i\delta t}+\Omega_1^-e^{-i\delta t} \\ 0 & \Delta_2 & \Omega_2^+e^{i\delta t}+\Omega_2^-e^{-i\delta t} \\ \bar{\Omega}_1^+e^{-i\delta t}+\bar{\Omega}_1^-e^{i\delta t} & \bar{\Omega}_2^+e^{-i\delta t}+\bar{\Omega}_2^-e^{i\delta t} & 0 \end{bmatrix}, \tag{1}$$

where $\Delta_1=\omega_{13}-\omega_a$ and $\Delta_2=\omega_{23}-\omega_b$ denote the detunings between the atomic transition frequencies and center frequencies of the fields. $\Omega_1^{\pm}(\Omega_2^{\pm})$ are the complex Rabi frequen-

cies defined as $\Omega_1^{\pm}=\frac{1}{2}\tilde{E}_a^{\pm}\mu_{13}$ and $\Omega_2^{\pm}=\frac{1}{2}\tilde{E}_b^{\pm}\mu_{23}$, where μ_{13} and μ_{23} are the electric dipole moments (real numbers) of the corresponding atomic transitions. $\bar{\Omega}_1^{\pm}$ and $\bar{\Omega}_2^{\pm}$ represent the complex conjugates of $\Omega_1^{\pm}$ and $\Omega_2^{\pm}$, respectively.

B. Master equation

Assuming that the system under consideration is closed (that is, the norm of the total wave function is conserved to unity), the system behavior can be described by the master equation which is derived from the reversible Liouville equation (i.e., $\dot{\rho}=1/i\hbar[H,\rho]$) together with the irreversible relaxation parameters:

$$\dot{x}(t)=(A_-e^{-i\delta t}+A_0+A_+e^{i\delta t})x(t)+e^{-i\delta t}\cdot V_-+e^{i\delta t}\cdot V_+. \tag{2}$$

In Eq. (2), A_+, A_0, and A_- are 8×8 matrices, and $x(t)$ and V_-, V_+ are 8×1 column vectors defined as follows:

$$x(t)=\begin{bmatrix}x_1(t)\\x_2(t)\\x_3(t)\\x_4(t)\\x_5(t)\\x_6(t)\\x_7(t)\\x_8(t)\end{bmatrix}=\begin{bmatrix}\rho_{32}\\\rho_{31}\\\rho_{23}\\\rho_{22}\\\rho_{21}\\\rho_{13}\\\rho_{12}\\\rho_{11}\end{bmatrix},\quad V_+=\begin{bmatrix}i\bar{\Omega}_2^-\\i\bar{\Omega}_1^-\\-i\Omega_2^+\\0\\0\\-i\Omega_1^+\\0\\0\end{bmatrix},\quad V_-=\begin{bmatrix}i\bar{\Omega}_2^+\\i\bar{\Omega}_1^+\\-i\Omega_2^-\\0\\0\\-i\Omega_1^-\\0\\0\end{bmatrix},$$

$$A_0=\mathrm{diag}[i\Delta_2-\gamma_{23},i\Delta_1-\gamma_{13},-i\Delta_2-\gamma_{23},-\Gamma_{22},i(\Delta_1-\Delta_2)-\gamma_{12},-i\Delta_1-\gamma_{13},i(\Delta_2-\Delta_1)-\gamma_{12},-\Gamma_{11}],$$

$$A_+=\begin{bmatrix}0&0&0&-2i\bar{\Omega}_2^-&0&0&-i\bar{\Omega}_1^-&-i\bar{\Omega}_2^-\\0&0&0&-i\bar{\Omega}_1^-&-i\bar{\Omega}_2^-&0&0&-2i\bar{\Omega}_1^-\\0&0&0&2i\Omega_2^+&i\Omega_1^+&0&0&i\Omega_2^+\\-i\Omega_2^+&0&i\bar{\Omega}_2^-&0&0&0&0&0\\0&-i\Omega_2^+&i\bar{\Omega}_1^-&0&0&0&0&0\\0&0&0&i\Omega_1^+&0&0&i\Omega_2^+&2i\Omega_1^+\\-i\Omega_1^+&0&0&0&0&i\bar{\Omega}_2^-&0&0\\0&-i\Omega_1^+&0&0&0&i\bar{\Omega}_1^-&0&0\end{bmatrix},$$

$$A_-=\begin{bmatrix}0&0&0&-2i\bar{\Omega}_2^+&0&0&-i\bar{\Omega}_1^+&-i\bar{\Omega}_2^+\\0&0&0&-i\bar{\Omega}_1^+&-i\bar{\Omega}_2^+&0&0&-2i\bar{\Omega}_1^+\\0&0&0&2i\Omega_2^-&i\Omega_1^-&0&0&i\Omega_2^-\\-i\Omega_2^-&0&i\bar{\Omega}_2^+&0&0&0&0&0\\0&-i\Omega_2^-&i\bar{\Omega}_1^+&0&0&0&0&0\\0&0&0&i\Omega_1^-&0&0&i\Omega_2^-&2i\Omega_1^-\\-i\Omega_1^-&0&0&0&0&i\bar{\Omega}_2^+&0&0\\0&-i\Omega_1^-&0&0&0&i\bar{\Omega}_1^+&0&0\end{bmatrix}.$$

In the equation for $x(t)$, the density matrix elements have been defined in the rotating-wave frame. $\Gamma_{11}(\Gamma_{22})$ denotes the spontaneous decay rate from the excited state $|1\rangle(|2\rangle)$ to the common ground state $|3\rangle$. Parameters γ_{13}, γ_{23}, γ_{12} are the damping rates of atomic coherences. If the spontaneous emission is the only relaxation mechanism, $\gamma_{12}=(\Gamma_{11}+\Gamma_{22})/2$, $\gamma_{13}=\Gamma_{11}/2$, and $\gamma_{23}=\Gamma_{22}/2$.

Since the Hamiltonian is periodical, the solution to Eq. (2) can be decomposed into harmonics, according to the Floquet theorem, with slowly varying envelopes:

$$x(t)=\sum_{n=-\infty}^{\infty}x^{(n)}(t)e^{in\delta t}. \tag{3}$$

Substituting Eq. (3) into Eq. (2), and applying the Laplace transform, we obtain the iterative relation below:

$$[(z+in\delta)I-A_0]\tilde{x}^{(n)}(z)-A_-\tilde{x}^{(n+1)}(z)-A_+\tilde{x}^{(n-1)}(z)$$
$$=x^{(n)}(t_0)+\frac{1}{z}(V_+\delta_{n,1}+V_-\delta_{n,-1}), \tag{4}$$

where $\delta_{n,1}$ and $\delta_{n,-1}$ are the Kronecker delta, I the 8×8 identity matrix, and $\tilde{x}^{(n)}(z)$ the Laplace transform of $x^{(n)}(t)$. (In the following we abide the convention that tilde is used for the Laplace transform of any time-dependent variable.) More explicitly Eq. (4) can be rewritten in a "supermatrix" form with an infinite dimension:

$$\begin{bmatrix} \cdots & \cdots & \cdots & \cdots & \cdots & \cdots & \cdots \\ -A_+ & M_{-2} & -A_- & 0 & 0 & 0 & 0 \\ 0 & -A_+ & M_{-1} & -A_- & 0 & 0 & 0 \\ 0 & 0 & -A_+ & M_0 & -A_- & 0 & 0 \\ 0 & 0 & 0 & -A_+ & M_1 & -A_- & 0 \\ 0 & 0 & 0 & 0 & -A_+ & M_2 & -A_- \\ \cdots & \cdots & \cdots & \cdots & \cdots & \cdots & \cdots \end{bmatrix} \begin{bmatrix} \cdots \\ \tilde{x}^{(-2)}(z) \\ \tilde{x}^{(-1)}(z) \\ \tilde{x}^{(0)}(z) \\ \tilde{x}^{(1)}(z) \\ \tilde{x}^{(2)}(z) \\ \cdots \end{bmatrix}$$
$$=\begin{bmatrix} \cdots \\ x^{(-2)}(t_0) \\ x^{(-1)}(t_0) \\ x^{(0)}(t_0) \\ x^{(1)}(t_0) \\ x^{(2)}(t_0) \\ \cdots \end{bmatrix}+\frac{1}{z}\begin{bmatrix} \cdots \\ 0 \\ V_- \\ 0 \\ V_+ \\ 0 \\ \cdots \end{bmatrix}, \tag{5}$$

where $M_n=(z+in\delta t)I-A_0$. Recalling that $x^{(n)}(t\to\infty)=\lim_{z\to 0}z\tilde{x}^{(n)}(z)$ from the complex function theory, the steady state value of $x^{(n)}(t)$ can be determined from Eq. (5) as

$$\begin{bmatrix} \cdots \\ x^{(-2)}(\infty) \\ x^{(-1)}(\infty) \\ x^{(0)}(\infty) \\ x^{(1)}(\infty) \\ x^{(2)}(\infty) \\ \cdots \end{bmatrix}$$
$$=\begin{bmatrix} \cdots & \cdots & \cdots & \cdots & \cdots & \cdots & \cdots \\ -A_+ & M_{-2}^{z=0} & -A_- & 0 & 0 & 0 & 0 \\ 0 & -A_+ & M_{-1}^{z=0} & -A_- & 0 & 0 & 0 \\ 0 & 0 & -A_+ & M_0^{z=0} & -A_- & 0 & 0 \\ 0 & 0 & 0 & -A_+ & M_1^{z=0} & -A_- & 0 \\ 0 & 0 & 0 & 0 & -A_+ & M_2^{z=0} & -A_- \\ \cdots & \cdots & \cdots & \cdots & \cdots & \cdots & \cdots \end{bmatrix}^{-1}$$
$$\cdot\begin{bmatrix} \cdots \\ 0 \\ V_- \\ 0 \\ V_+ \\ 0 \\ \cdots \end{bmatrix}, \tag{6}$$

where $M_n^{z=0}=in\delta tI-A_0$. Now the steady state populations and coherences of the three-level atom can be numerically calculated from Eq. (6) by truncating the harmonic expansion of $x(t)$ at a certain order which is sufficiently large for the numerical convergence.

For the convenience of quantum regression theorem to be used later on, we go back to the non-rotating-wave frame and introduce an 8×1 vector, $X(t)$, in which each component can be obtained from that of $x(t)$ multiplied by the corresponding free evolution term:

$$X(t)=\begin{bmatrix} X_1(t) \\ X_2(t) \\ X_3(t) \\ X_4(t) \\ X_5(t) \\ X_6(t) \\ X_7(t) \\ X_8(t) \end{bmatrix}=\begin{bmatrix} \langle|2\rangle\langle 3|\rangle_t \\ \langle|1\rangle\langle 3|\rangle_t \\ \langle|3\rangle\langle 2|\rangle_t \\ \langle|2\rangle\langle 2|\rangle_t \\ \langle|1\rangle\langle 2|\rangle_t \\ \langle|3\rangle\langle 1|\rangle_t \\ \langle|2\rangle\langle 1|\rangle_t \\ \langle|1\rangle\langle 1|\rangle_t \end{bmatrix}=\begin{bmatrix} x_1(t)e^{i\omega_b(t-t_0)} \\ x_2(t)e^{i\omega_a(t-t_0)} \\ x_3(t)e^{-i\omega_b(t-t_0)} \\ x_4(t) \\ x_5(t)e^{i(\omega_a-\omega_b)(t-t_0)} \\ x_6(t)e^{-i\omega_a(t-t_0)} \\ x_7(t)e^{-i(\omega_a-\omega_b)(t-t_0)} \\ x_8(t) \end{bmatrix} \tag{7}$$

and accordingly,

$$X(z) = \begin{bmatrix} \tilde{X}_1(z + i\omega_b) \\ \tilde{X}_2(z + i\omega_a) \\ \tilde{X}_3(z - i\omega_b) \\ \tilde{X}_4(z) \\ \tilde{X}_5[z + i(\omega_a - \omega_b)] \\ \tilde{X}_6(z - i\omega_a) \\ \tilde{X}_7[z - i(\omega_a - \omega_b)] \\ \tilde{X}_8(z) \end{bmatrix} = \begin{bmatrix} \tilde{x}_1(z) \\ \tilde{x}_2(z) \\ \tilde{x}_3(z) \\ \tilde{x}_4(z) \\ \tilde{x}_5(z) \\ \tilde{x}_6(z) \\ \tilde{x}_7(z) \\ \tilde{x}_8(z) \end{bmatrix}. \quad (8)$$

By expanding $X(t)$ in terms of the harmonics as before,

$$X(t) = \sum_{n=-\infty}^{\infty} X^{(n)}(t) e^{in\delta t} \quad (9)$$

we arrive at the following equation which is the main analytical result to calculate the fluorescence and absorption:

$$\begin{bmatrix} \cdots & \cdots & \cdots & \cdots & \cdots & \cdots & \cdots \\ -A_+ & M_{-2} & -A_- & 0 & 0 & 0 & 0 \\ 0 & -A_+ & M_{-1} & -A_- & 0 & 0 & 0 \\ 0 & 0 & -A_+ & M_0 & -A_- & 0 & 0 \\ 0 & 0 & 0 & -A_+ & M_1 & -A_- & 0 \\ 0 & 0 & 0 & 0 & -A_+ & M_2 & -A_- \\ \cdots & \cdots & \cdots & \cdots & \cdots & \cdots & \cdots \end{bmatrix} \begin{bmatrix} \cdots \\ \tilde{X}^{(-2)}(z) \\ \tilde{X}^{(-1)}(z) \\ \tilde{X}^{(0)}(z) \\ \tilde{X}^{(1)}(z) \\ \tilde{X}^{(2)}(z) \\ \cdots \end{bmatrix}$$
$$= \begin{bmatrix} \cdots \\ x^{(-2)}(t_0) \\ x^{(-1)}(t_0) \\ x^{(0)}(t_0) \\ x^{(1)}(t_0) \\ x^{(2)}(t_0) \\ \cdots \end{bmatrix} + \frac{1}{z} \begin{bmatrix} \cdots \\ 0 \\ V_- \\ 0 \\ V_+ \\ 0 \\ \cdots \end{bmatrix}. \quad (10)$$

C. Fluorescence spectrum

Having obtained the above formula for the atomic response, we proceed further to calculate the spectrum. The fluorescence spectrum is computed from the real part of the unilateral Fourier transform of the two-time dipole correlation function [2]. In our three-level atom, the fluorescence spectra can be divided into two frequency ranges, each of which corresponds to one of the atomic dipole transitions, $|1\rangle \leftrightarrow |3\rangle$ and $|2\rangle \leftrightarrow |3\rangle$. Thus, the total fluorescence spectra are obtained from the following relations:

$${}^1G(\omega) = \mu_{13}{}^2 \mathrm{Re}\left\{ \int_0^{+\infty} [\langle P_1^+(t) P_1^-(t_0)\rangle] e^{i\omega t} dt \right\}, \quad (11a)$$

$${}^2G(\omega) = \mu_{23}{}^2 \mathrm{Re}\left\{ \int_0^{+\infty} [\langle P_2^+(t) P_2^-(t_0)\rangle] e^{i\omega t} dt \right\}, \quad (11b)$$

where

$$P_1^+(t) \equiv |1\rangle\langle 3|_t, P_1^-(t_0) \equiv |3\rangle\langle 1|_{t_0},$$

$$P_2^+(t) \equiv |2\rangle\langle 3|_t, \quad P_2^-(t_0) \equiv |3\rangle\langle 2|_{t_0}. \quad (12)$$

Integrating the fluorescence spectrum over the full frequency domain yields the total fluorescence intensity corresponding to each of the atomic transitions, i.e., ${}^1I_{total} = \int_{-\infty}^{\infty} {}^1G(\omega) d\omega$ and ${}^2I_{total} = \int_{-\infty}^{\infty} {}^2G(\omega) d\omega$, respectively. However, we calculate the total fluorescence intensities with an alternative approach, which is simply in terms of the steady state populations of the excited states, i.e., ${}^1I_{total} = \mu_{13}{}^2 x_8^{(0)}(\infty)$ and ${}^2I_{total} = \mu_{23}{}^2 x_4^{(0)}(\infty)$. Conveniently the fluorescence spectrum is divided into the two contributions, i.e., inelastic and elastic parts, i.e., ${}^1G(\omega) = {}^1G_{in}(\omega) + {}^1G_{el}(\omega)$ and ${}^2G(\omega) = {}^2G_{in}(\omega) + {}^2G_{el}(\omega)$. The elastic part of the spectrum can be computed from the following equations:

$${}^1G_{el}(\omega) = \mu_{13}^2 \mathrm{Re}\left[\int_0^{+\infty} \langle P_1^+(t)\rangle\langle P_1^-(t_0)\rangle e^{i\omega t} dt \right] \quad (13a)$$

$${}^2G_{el}(\omega) = \mu_{23}^2 \mathrm{Re}\left[\int_0^{+\infty} \langle P_2^+(t)\rangle\langle P_2^-(t_0)\rangle e^{i\omega t} dt \right] \quad (13b)$$

which, in the steady state, simply yields

$${}^1G_{el}(\omega) = \mu_{13}^2 \sum_{m=-\infty}^{\infty} |x_2^{(m)}(\infty)|^2 \hat{\delta}(\omega - \omega_a - m\delta), \quad (14a)$$

$${}^2G_{el}(\omega) = \mu_{23}^2 \sum_{m=-\infty}^{\infty} |x_1^{(m)}(\infty)|^2 \hat{\delta}(\omega - \omega_b - m\delta), \quad (14b)$$

where $\hat{\delta}$ denotes the Dirac delta function. (Note that, although the elastic part of the fluorescence theoretically has a zero linewidth, it is not so in practice due to the limited spectral resolution and the finite linewidths of the driving fields.) The total elastic intensity can be obtained by directly summing up all elastic terms in Eq. (14), therefore we have ${}^1I_{total}^{el} = \mu_{13}{}^2 \Sigma_{m=-\infty}^{\infty} |x_2^{(m)}(\infty)|^2$ and ${}^2I_{total}^{el} = \mu_{23}{}^2 \Sigma_{m=-\infty}^{\infty} |x_1^{(m)}(\infty)|^2$. The inelastic part of the spectrum, ${}^1G_{in}(\omega)$ and ${}^2G_{in}(\omega)$, which is also termed as incoherent fluorescence in the following discussions, is obtained simply by using ${}^1G_{in}(\omega) = {}^1G(\omega) - {}^1G_{el}(\omega)$ and ${}^1G_{in}(\omega) = {}^1G(\omega) - {}^1G_{el}(\omega)$, i.e.,

$${}^1G_{in}(\omega) = \mu_{13}^2 \mathrm{Re}\left\{ \int_0^{+\infty} [\langle P_1^+(t) P_1^-(t_0)\rangle - \langle P_1^+(t)\rangle\langle P_1^-(t_0)\rangle] e^{i\omega t} dt \right\}, \quad (15a)$$

$$^2G_{in}(\omega) = \mu_{23}^2 \mathrm{Re}\left\{\int_0^{+\infty} [\langle P_2^+(t)P_2^-(t_0)\rangle - \langle P_2^+(t)\rangle\langle P_2^-(t_0)\rangle]e^{i\omega t}dt\right\}. \tag{15b}$$

In order to calculate the incoherent fluorescence spectrum, we need to invoke quantum regression theorem and for convenience introduce the following vectors, $^1Y(t)$ and $^2Y(t)$:

$$^1Y(t) = \begin{bmatrix} ^1Y_1(t) \\ ^1Y_2(t) \\ ^1Y_3(t) \\ ^1Y_4(t) \\ ^1Y_5(t) \\ ^1Y_6(t) \\ ^1Y_7(t) \\ ^1Y_8(t) \end{bmatrix} = \begin{bmatrix} \langle|2\rangle\langle 3|_t P_1^-(t_0)\rangle - \langle|2\rangle\langle 3|\rangle_t\langle P_1^-(t_0)\rangle \\ \langle|1\rangle\langle 3|_t P_1^-(t_0)\rangle - \langle|1\rangle\langle 3|\rangle_t\langle P_1^-(t_0)\rangle \\ \langle|3\rangle\langle 2|_t P_1^-(t_0)\rangle - \langle|3\rangle\langle 2|\rangle_t\langle P_1^-(t_0)\rangle \\ \langle|2\rangle\langle 2|_t P_1^-(t_0)\rangle - \langle|2\rangle\langle 2|\rangle_t\langle P_1^-(t_0)\rangle \\ \langle|1\rangle\langle 2|_t P_1^-(t_0)\rangle - \langle|1\rangle\langle 2|\rangle_t\langle P_1^-(t_0)\rangle \\ \langle|3\rangle\langle 1|_t P_1^-(t_0)\rangle - \langle|3\rangle\langle 1|\rangle_t\langle P_1^-(t_0)\rangle \\ \langle|2\rangle\langle 1|_t P_1^-(t_0)\rangle - \langle|2\rangle\langle 1|\rangle_t\langle P_1^-(t_0)\rangle \\ \langle|1\rangle\langle 1|_t P_1^-(t_0)\rangle - \langle|1\rangle\langle 1|\rangle_t\langle P_1^-(t_0)\rangle \end{bmatrix}, \tag{16a}$$

$$^2Y(t) = \begin{bmatrix} ^2Y_1(t) \\ ^2Y_2(t) \\ ^2Y_3(t) \\ ^2Y_4(t) \\ ^2Y_5(t) \\ ^2Y_6(t) \\ ^2Y_7(t) \\ ^2Y_8(t) \end{bmatrix} = \begin{bmatrix} \langle|2\rangle\langle 3|_t P_2^-(t_0)\rangle - \langle|2\rangle\langle 3|\rangle_t\langle P_2^-(t_0)\rangle \\ \langle|1\rangle\langle 3|_t P_2^-(t_0)\rangle - \langle|1\rangle\langle 3|\rangle_t\langle P_2^-(t_0)\rangle \\ \langle|3\rangle\langle 2|_t P_2^-(t_0)\rangle - \langle|3\rangle\langle 2|\rangle_t\langle P_2^-(t_0)\rangle \\ \langle|2\rangle\langle 2|_t P_2^-(t_0)\rangle - \langle|2\rangle\langle 2|\rangle_t\langle P_2^-(t_0)\rangle \\ \langle|1\rangle\langle 2|_t P_2^-(t_0)\rangle - \langle|1\rangle\langle 2|\rangle_t\langle P_2^-(t_0)\rangle \\ \langle|3\rangle\langle 1|_t P_2^-(t_0)\rangle - \langle|3\rangle\langle 1|\rangle_t\langle P_2^-(t_0)\rangle \\ \langle|2\rangle\langle 1|_t P_2^-(t_0)\rangle - \langle|2\rangle\langle 1|\rangle_t\langle P_2^-(t_0)\rangle \\ \langle|1\rangle\langle 1|_t P_2^-(t_0)\rangle - \langle|1\rangle\langle 1|\rangle_t\langle P_2^-(t_0)\rangle \end{bmatrix}. \tag{16b}$$

$^1Y(t)$, $^2Y(t)$ can also be expanded in Fourier series:

$$^1Y(t) = \sum_{n=-\infty}^{\infty} {}^1Y^{(n)}(t)e^{in\delta t}, \quad ^2Y(t) = \sum_{n=-\infty}^{\infty} {}^2Y^{(n)}(t)e^{in\delta t} \tag{17a}$$

and their initial values at $t=t_0$ are specified as

$$^1Y(t_0) = \sum_{n=-\infty}^{\infty} {}^1Y^{(n)}(t_0)e^{in\delta t_0}, \quad ^2Y(t_0) = \sum_{n=-\infty}^{\infty} {}^2Y^{(n)}(t_0)e^{in\delta t_0}. \tag{17b}$$

Each component of $^1Y(t)$, $^2Y(t)$ represents a two-time atomic dipole correlation function. From quantum regression theorem, we know that, with properly defined initial values, $^1\tilde{Y}(z)$, $^2\tilde{Y}(z)$ [the Laplace transform of $^1Y(t)$, $^2Y(t)$] obey the same evolution equation as $\tilde{X}(z)$. To be explicit, by substituting $\tilde{X}(z)$ with $^1\tilde{Y}(z)$, $^2\tilde{Y}(z)$,$X(t_0)$ with $^1Y(t_0)$, $^2Y(t_0)$, and dropping the inhomogeneous term in Eq. (10), we have the evolution equation of $^1\tilde{Y}(z)$, $^2\tilde{Y}(z)$. Furthermore, since we are interested in the steady state spectrum, the initial values $^1Y(t_0)$ and $^2Y(t_0)$ should be taken at the steady state limit, $^1Y(\infty)$, $^2Y(\infty)$. Thus we obtain

$$\begin{bmatrix} \cdots & \cdots & \cdots & \cdots & \cdots & \cdots & \cdots \\ -A_+ & M_{-2} & -A_- & 0 & 0 & 0 & 0 \\ 0 & -A_+ & M_{-1} & -A_- & 0 & 0 & 0 \\ 0 & 0 & -A_+ & M_0 & -A_- & 0 & 0 \\ 0 & 0 & 0 & -A_+ & M_1 & -A_- & 0 \\ 0 & 0 & 0 & 0 & -A_+ & M_2 & -A_- \\ \cdots & \cdots & \cdots & \cdots & \cdots & \cdots & \cdots \end{bmatrix} \begin{bmatrix} \cdots \\ {}^1\tilde{Y}^{(-2)}(z) \\ {}^1\tilde{Y}^{(-1)}(z) \\ {}^1\tilde{Y}^{(0)}(z) \\ {}^1\tilde{Y}^{(1)}(z) \\ {}^1\tilde{Y}^{(2)}(z) \\ \cdots \end{bmatrix} = \begin{bmatrix} \cdots \\ {}^1Y^{(-2)}(\infty) \\ {}^1\tilde{Y}^{(-1)}(\infty) \\ {}^1Y^{(0)}(\infty) \\ {}^1Y^{(1)}(\infty) \\ {}^1Y^{(2)}(\infty) \\ \cdots \end{bmatrix}, \tag{18a}$$

$$\begin{bmatrix} \cdots & \cdots & \cdots & \cdots & \cdots & \cdots & \cdots \\ -A_+ & M_{-2} & -A_- & 0 & 0 & 0 & 0 \\ 0 & -A_+ & M_{-1} & -A_- & 0 & 0 & 0 \\ 0 & 0 & -A_+ & M_0 & -A_- & 0 & 0 \\ 0 & 0 & 0 & -A_+ & M_1 & -A_- & 0 \\ 0 & 0 & 0 & 0 & -A_+ & M_2 & -A_- \\ \cdots & \cdots & \cdots & \cdots & \cdots & \cdots & \cdots \end{bmatrix} \begin{bmatrix} \cdots \\ {}^2\tilde{Y}^{(-2)}(z) \\ {}^1\tilde{Y}^{(-2)}(z) \\ {}^1\tilde{Y}^{(0)}(z) \\ {}^2\tilde{Y}^{(1)}(z) \\ {}^2\tilde{Y}^{(2)}(z) \\ \cdots \end{bmatrix} = \begin{bmatrix} \cdots \\ {}^2Y^{(-2)}(\infty) \\ {}^1\tilde{Y}^{(-2)}(\infty) \\ {}^1Y^{(0)}(\infty) \\ {}^2Y^{(1)}(\infty) \\ {}^2Y^{(2)}(\infty) \\ \cdots \end{bmatrix}. \tag{18b}$$

The right-hand sides of Eqs. (18a) and (18b) are determined after straightforward manipulation:

$$^1Y^{(n)}(\infty) = \begin{bmatrix} x_7^{(n)}(\infty) \\ x_8^{(n)}(\infty) \\ 0 \\ 0 \\ 0 \\ 0 \\ 0 \end{bmatrix} - \sum_{m=-\infty}^{\infty} \begin{bmatrix} x_1^{(m)}(\infty)x_6^{(n-m)}(\infty) \\ x_2^{(m)}(\infty)x_6^{(n-m)}(\infty) \\ x_3^{(m)}(\infty)x_6^{(n-m)}(\infty) \\ x_4^{(m)}(\infty)x_6^{(n-m)}(\infty) \\ x_5^{(m)}(\infty)x_6^{(n-m)}(\infty) \\ x_6^{(m)}(\infty)x_6^{(n-m)}(\infty) \\ x_7^{(m)}(\infty)x_6^{(n-m)}(\infty) \\ x_8^{(m)}(\infty)x_6^{(n-m)}(\infty) \end{bmatrix}, \tag{19a}$$

$$ {}^2Y^{(n)}(\infty) = \begin{bmatrix} x_4^{(n)}(\infty) \\ x_5^{(n)}(\infty) \\ 0 \\ 0 \\ 0 \\ 0 \\ 0 \end{bmatrix} - \sum_{m=-\infty}^{\infty} \begin{bmatrix} x_1^{(m)}(\infty)x_3^{(n-m)}(\infty) \\ x_2^{(m)}(\infty)x_3^{(n-m)}(\infty) \\ x_3^{(m)}(\infty)x_3^{(n-m)}(\infty) \\ x_4^{(m)}(\infty)x_3^{(n-m)}(\infty) \\ x_5^{(m)}(\infty)x_3^{(n-m)}(\infty) \\ x_6^{(m)}(\infty)x_3^{(n-m)}(\infty) \\ x_7^{(m)}(\infty)x_3^{(n-m)}(\infty) \\ x_8^{(m)}(\infty)x_3^{(n-m)}(\infty) \end{bmatrix}. \tag{19b} $$

Since all steady state values in Eq. (19) have been obtained from Eq. (6), Eq. (18) can be numerically calculated without ambiguity. Then the incoherent fluorescence spectrum in steady state is simply

$$ \begin{aligned} S_{in}(\omega) &= {}^1G_{in}(\omega) + {}^2G_{in}(\omega) \\ &= {}^1Y_2^{(0)}(z)|_{z=i(\omega-\omega_a)} + {}^2Y_1^{(0)}(z)|_{z=i(\omega-\omega_b)}. \end{aligned} \tag{20} $$

D. Absorption spectrum

As proposed by the linear response theory [1], the absorption spectrum of a weak monochromatic field probing an atomic transition is defined in terms of the two-time commutator of the atomic lowering and raising operators. Since there are two dipole transitions in our three-level atom, we divide the absorption spectrum into two frequency ranges, as we have done for the fluorescence spectrum:

$$ {}^1W(\omega) = \mu_{13}^2 \mathrm{Re} \int_0^{+\infty} \langle P_1^-(t_0)P_1^+(t) - P_1^+(t)P_1^-(t_0)\rangle e^{i\omega t} dt, \tag{21a} $$

$$ {}^2W(\omega) = \mu_{23}^2 \mathrm{Re} \int_0^{+\infty} \langle P_2^-(t_0)P_2^+(t) - P_2^+(t)P_2^-(t_0)\rangle e^{i\omega t} dt. \tag{21b} $$

Again, as in the manipulation of the fluorescence spectrum, we introduce two column vectors:

$$ {}^1U(t) = \begin{bmatrix} {}^1U_1(t) \\ {}^1U_2(t) \\ {}^1U_3(t) \\ {}^1U_4(t) \\ {}^1U_5(t) \\ {}^1U_6(t) \\ {}^1U_7(t) \\ {}^1U_8(t) \end{bmatrix} = \begin{bmatrix} \langle P_1^-(t_0)|2\rangle\langle 3|_t\rangle - \langle|2\rangle\langle 3|_t P_1^-(t_0)\rangle \\ \langle P_1^-(t_0)|1\rangle\langle 3|_t\rangle - \langle|1\rangle\langle 3|_t P_1^-(t_0)\rangle \\ \langle P_1^-(t_0)|3\rangle\langle 2|_t\rangle - \langle|3\rangle\langle 2|_t P_1^-(t_0)\rangle \\ \langle P_1^-(t_0)|2\rangle\langle 2|_t\rangle - \langle|2\rangle\langle 2|_t P_1^-(t_0)\rangle \\ \langle P_1^-(t_0)|1\rangle\langle 2|_t\rangle - \langle|1\rangle\langle 2|_t P_1^-(t_0)\rangle \\ \langle P_1^-(t_0)|3\rangle\langle 1|_t\rangle - \langle|3\rangle\langle 1|_t P_1^-(t_0)\rangle \\ \langle P_1^-(t_0)|2\rangle\langle 1|_t\rangle - \langle|2\rangle\langle 1|_t P_1^-(t_0)\rangle \\ \langle P_1^-(t_0)|1\rangle\langle 1|_t\rangle - \langle|1\rangle\langle 1|_t P_1^-(t_0)\rangle \end{bmatrix}, \tag{22a} $$

$$ {}^2U(t) = \begin{bmatrix} {}^2U_1(t) \\ {}^2U_2(t) \\ {}^2U_3(t) \\ {}^2U_4(t) \\ {}^2U_5(t) \\ {}^2U_6(t) \\ {}^2U_7(t) \\ {}^2U_8(t) \end{bmatrix} = \begin{bmatrix} \langle P_2^-(t_0)|2\rangle\langle 3|_t\rangle - \langle|2\rangle\langle 3|_t P_2^-(t_0)\rangle \\ \langle P_2^-(t_0)|1\rangle\langle 3|_t\rangle - \langle|1\rangle\langle 3|_t P_2^-(t_0)\rangle \\ \langle P_2^-(t_0)|3\rangle\langle 2|_t\rangle - \langle|3\rangle\langle 2|_t P_2^-(t_0)\rangle \\ \langle P_2^-(t_0)|2\rangle\langle 2|_t\rangle - \langle|2\rangle\langle 2|_t P_2^-(t_0)\rangle \\ \langle P_2^-(t_0)|1\rangle\langle 2|_t\rangle - \langle|1\rangle\langle 2|_t P_2^-(t_0)\rangle \\ \langle P_2^-(t_0)|3\rangle\langle 1|_t\rangle - \langle|3\rangle\langle 1|_t P_2^-(t_0)\rangle \\ \langle P_2^-(t_0)|2\rangle\langle 1|_t\rangle - \langle|2\rangle\langle 1|_t P_2^-(t_0)\rangle \\ \langle P_2^-(t_0)|1\rangle\langle 1|_t\rangle - \langle|1\rangle\langle 1|_t P_2^-(t_0)\rangle \end{bmatrix}. \tag{22b} $$

${}^1U(t)$, ${}^2U(t)$ can also be expanded in Fourier series:

$$ {}^1U(t) = \sum_{n=-\infty}^{\infty} {}^1U^{(n)}(t)e^{in\delta t}, \quad {}^2U(t) = \sum_{n=-\infty}^{\infty} {}^2U^{(n)}(t)e^{in\delta t} \tag{23a} $$

and their initial value at $t=t_0$ are specified as

$$ {}^1U(t_0) = \sum_{n=-\infty}^{\infty} {}^1U^{(n)}(t_0)e^{in\delta t_0}, \quad {}^2U(t_0) = \sum_{n=-\infty}^{\infty} {}^2U^{(n)}(t_0)e^{in\delta t_0}. \tag{23b} $$

Invoking quantum regression theorem and following a similar procedure as in the fluorescence spectrum, the Laplace transform of ${}^1U(t)$, ${}^2U(t)$ can be obtained as

$$ \begin{bmatrix} \cdots & \cdots & \cdots & \cdots & \cdots & \cdots & \cdots \\ -A_+ & M_{-2} & -A_- & 0 & 0 & 0 & 0 \\ 0 & -A_+ & M_{-1} & -A_- & 0 & 0 & 0 \\ 0 & 0 & -A_+ & M_0 & -A_- & 0 & 0 \\ 0 & 0 & 0 & -A_+ & M_1 & -A_- & 0 \\ 0 & 0 & 0 & 0 & -A_+ & M_2 & -A_- \\ \cdots & \cdots & \cdots & \cdots & \cdots & \cdots & \cdots \end{bmatrix} \begin{bmatrix} \cdots \\ {}^1\tilde{U}^{(-2)}(z) \\ {}^1\tilde{U}^{(-1)}(z) \\ {}^1\tilde{U}^{(0)}(z) \\ {}^1\tilde{U}^{(1)}(z) \\ {}^1\tilde{U}^{(2)}(z) \\ \cdots \end{bmatrix} = \begin{bmatrix} \cdots \\ {}^1U^{(-2)}(\infty) \\ {}^1U^{(-1)}(\infty) \\ {}^1U^{(0)}(\infty) \\ {}^1U^{(1)}(\infty) \\ {}^1U^{(2)}(\infty) \\ \cdots \end{bmatrix}, \tag{24a} $$

$$\begin{bmatrix} \cdots & \cdots & \cdots & \cdots & \cdots & \cdots & \cdots \\ -A_+ & M_{-2} & -A_- & 0 & 0 & 0 & 0 \\ 0 & -A_+ & M_{-1} & -A_- & 0 & 0 & 0 \\ 0 & 0 & -A_+ & M_0 & -A_- & 0 & 0 \\ 0 & 0 & 0 & -A_+ & M_1 & -A_- & 0 \\ 0 & 0 & 0 & 0 & -A_+ & M_2 & -A_- \\ \cdots & \cdots & \cdots & \cdots & \cdots & \cdots & \cdots \end{bmatrix} \begin{bmatrix} \cdots \\ {}^2\tilde{U}^{(-2)}(z) \\ {}^2\tilde{U}^{(-1)}(z) \\ {}^2\tilde{U}^{(0)}(z) \\ {}^2\tilde{U}^{(1)}(z) \\ {}^2\tilde{U}^{(2)}(z) \\ \cdots \end{bmatrix}$$

$$= \begin{bmatrix} \cdots \\ {}^2U^{(-2)}(\infty) \\ {}^2U^{(-1)}(\infty) \\ {}^2U^{(0)}(\infty) \\ {}^2U^{(1)}(\infty) \\ {}^2U^{(2)}(\infty) \\ \cdots \end{bmatrix}, \tag{24b}$$

where

$${}^1U^{(n)}(\infty) = \begin{bmatrix} -x_7^{(n)}(\infty) \\ \delta_{n,0} - x_4^{(n)}(\infty) - 2x_8^{(n)}(\infty) \\ 0 \\ 0 \\ x_3^{(n)}(\infty) \\ 0 \\ 0 \\ x_6^{(n)}(\infty) \end{bmatrix},$$

$${}^2U^{(n)}(\infty) = \begin{bmatrix} \delta_{n,0} - 2x_4^{(n)}(\infty) - x_8^{(n)}(\infty) \\ -x_5^{(n)}(\infty) \\ 0 \\ x_3^{(n)}(\infty) \\ 0 \\ 0 \\ x_6^{(n)}(\infty) \\ 0 \end{bmatrix}. \tag{25}$$

Using Eqs. (6), (24), and (25), ${}^1\tilde{U}(z)$, ${}^2\tilde{U}(z)$ can be computed numerically by truncating the harmonic expansion at a certain order. Then the absorption spectrum in steady state is simply obtained as follows:

$$A(\omega) = {}^1W(\omega) + {}^2W(\omega) = {}^1U_2^{(0)}(z)\big|_{z=i(\omega-\omega_a)} + {}^2U_1^{(0)}(z)\big|_{z=i(\omega-\omega_b)}. \tag{26}$$

Note that the absorption spectrum is denoted by $A(\omega)$, which should not be confused with the coefficient matrices A_0 and $A_\pm$, used in Eq. (2).

III. NUMERICAL RESULTS AND DISCUSSION

Using Eqs. (6), (18)–(20), and (24)–(26) derived in the previous section, we can now calculate the fluorescence and absorption spectra. In all the numerical calculations presented in this section, we assume that the two frequency components of each bichromatic field have the same intensity and the corresponding *complex* Rabi frequencies are expressed as $\Omega_1^\pm = \Omega_1 \exp(i\theta_1^\pm)$ and $\Omega_2^\pm = \Omega_2 \exp(i\theta_2^\pm)$, with $\theta_{1,2}^\pm$ and $\Omega_{1,2}$ being the phase angles and the norms of the complex Rabi frequencies, respectively. Also, we define the relative phase $\Phi \equiv \frac{1}{2}[(\theta_2^+ - \theta_2^-) - (\theta_1^+ - \theta_1^-)]$, which is equivalent to the phase delay $\varphi_2 - \varphi_1$ between the modulating signals that we have explained in Sec. I. In the following sections we present some representative results focusing on the fluorescence and absorption spectra corresponding to the 1–3 transition with all the relevant parameters normalized with respect to Γ_{11}.

A. Effects of the second bichromatic field

First we investigate how much the fluorescence and absorption spectra corresponding to the 1–3 transition are affected by the introduction of the second bichromatic field, L_b. For a set of parameters $\delta=5$, $\Gamma_{22}=0.1$, $\Delta_1=\Delta_2=0$, and $\Omega_1=1$, the incoherent fluorescence and probe absorption spectra, and the total fluorescence intensity corresponding to the transition 1–3 are plotted in Figs. 2(a)–2(c), for the in-phase condition, i.e., $\Phi=0$, for several different values of Ω_2. Clearly the incoherent fluorescence spectrum [Fig. 2(a)] shows the following features: (1) The spectrum consists of a central peak and multiple side peaks with equidistant frequency spacing δ, and each peak has a Lorenzian shape under the secular approximation ($\delta \gg \Gamma_{11}$); (2) The intensity of each peak oscillates with Ω_2 and finally approaches zero as Ω_2 goes to infinity; (3) All peaks demonstrate remarkable line narrowing as Ω_2 increases. Further calculations (not shown here) show that, with the strong coupling field ($\Omega_2 \gg \Omega_1$), the widths of all even orders of side peaks (including the central peak) approach Γ_{22}, while those of all odd orders of side peaks approach $\frac{3}{2}\Gamma_{22}$. Similarly the probe absorption spectrum [Fig. 2(b)] also consists of a central peak and multiple equidistant side peaks and the intensity of each peak oscillates as Ω_2 increases. In contrast to the incoherent fluorescence spectrum in Fig. 2(a), no line-narrowing effect is observed in the absorption spectrum for all the *side peaks*. They have effective widths between Γ_{11} and $\Gamma_{11}+\Gamma_{22}$ for all values of Ω_2. For the *central peak*, its shape is not a simple Lorenzian and remarkable line-narrowing takes place at the Ω_2's where the peak is very small. For example, the *central peak* becomes much smaller than its neighboring side peaks for $\Omega_2=5$, and its effective width is reduced to about $0.2\Gamma_{11}$. After Ω_2 passes the first zero point ($\Omega_2 \approx 7$), the *central peak* recovers and its width approaches to Γ_{11} again at the next maximal position. The elastic fluorescence spectrum corresponding to the 1–3 transition was not presented in Fig. 2(a) since we are mainly interested in the line-narrowing effect which is obviously absent in the elastic fluorescence spectrum. Moreover, in order to see notable line narrowing, the

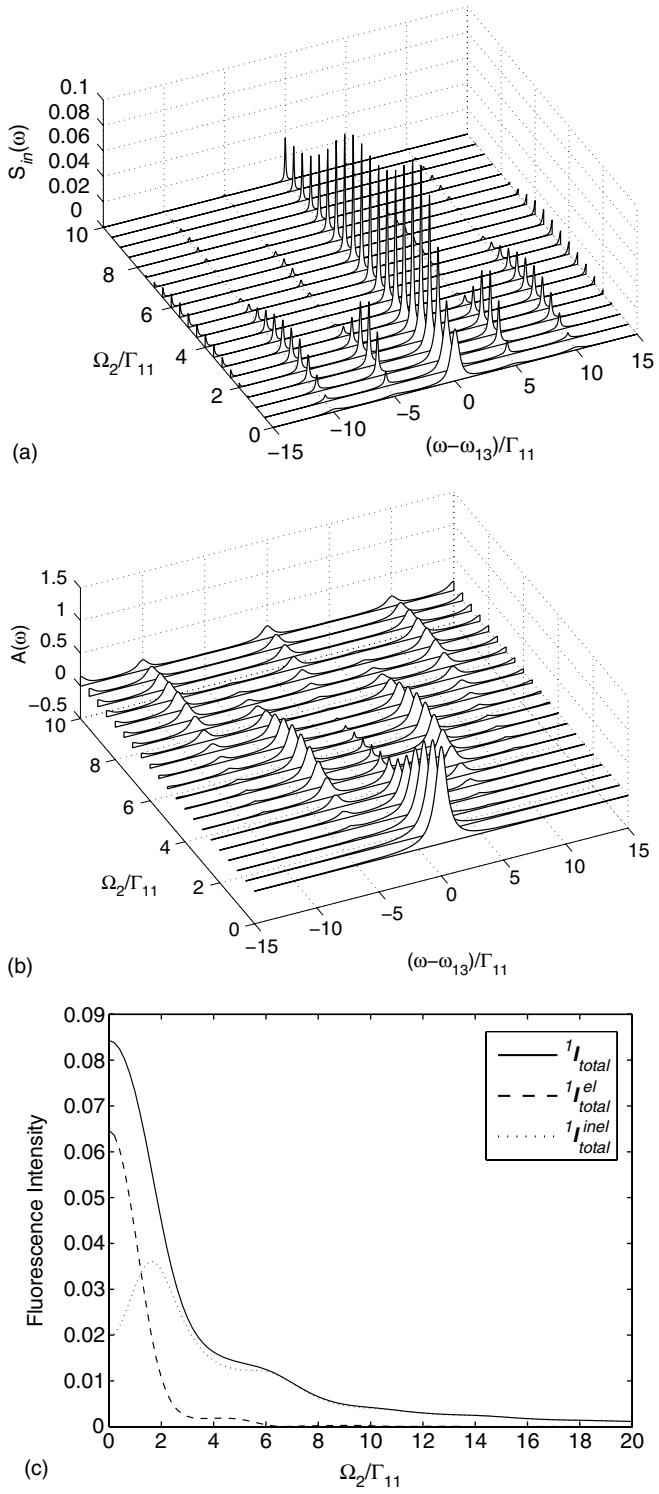

FIG. 2. (a) Incoherent fluorescence spectrum corresponding to the 1–3 transition, with $\delta=5$, $\Delta_1=\Delta_2=0$, $\Omega_1=1$, and $\Phi=0$. Note that the line narrowing takes place for each peak as Ω_2 increases. (b) Probe absorption spectrum corresponding to the 1–3 transition. All parameters are the same with those for graph (a). (c) Total fluorescence intensity corresponding to the 1–3 transition, plotted as a function of Ω_2. Solid, dashed, and dotted lines represent the total, elastic, and inelastic fluorescence intensities, respectively. All parameters are the same with those for graph (a).

value of Ω_2 must be sufficiently large, for which the contribution of the elastic process in the total fluorescence signal becomes negligibly small. This can be clearly seen in Fig. 2(c): At $\Omega_2>1.2$ intensity of the inelastic fluorescence becomes greater than the elastic fluorescence, and at $\Omega_2>6$ the elastic fluorescence intensity is less than 5% of the total fluorescence intensity. The apparent decrease of the total fluorescence intensity with respect to Ω_2 clearly manifests the "atomic shelving" effect, in which the population of state $|1\rangle$ is greatly reduced due to the strong coupling for the 2–3 transition. It should be noted that the elastic part of fluorescence only shows on odd multiples of δ, the presence of this elastic contribution effectively introduces an additional narrowing on the experimentally observed widths of the odd orders of side peaks. This may lead to a more or less deviation of the observed spectral widths from what we have calculated above, in which the impact of the elastic part of fluorescence on the observed spectral widths is neglected.

B. Effects of the phase delay between the two bichromatic fields

Next we examine how the spectrum is altered by changing the phase parameters $\theta^{\pm}_{1,2}$. Our calculations (not presented in this paper) show that the spectra depend only on the relative phase delay $\Phi\equiv\frac{1}{2}[(\theta_2^+-\theta_2^-)-(\theta_1^+-\theta_1^-)]$. In other words, if we set $\Phi=0$ as in the case of Fig. 2, the spectra do not depend on the individual variations of the phase angles $\theta^{\pm}_{1,2}$. In addition, we find that both fluorescence and absorption spectra are periodical functions of Φ with a period of π instead of 2π. This implies that the spectra actually depend on the phase delay between the envelopes of the *intensities*, rather than the *amplitudes*, of the two bichromatic fields. Representative results are shown in Fig. 3. In Fig. 3(a), we plot the incoherent fluorescence spectrum for several different values of Φ, with $\Omega_2=3$ and all other parameters remaining the same as in Fig. 2. As Φ increases from 0 to π, the incoherent fluorescence spectrum changes remarkably and the most pronounced phenomenon is the line splitting. As shown in Fig. 3(a), all even orders of side peaks split into doublets while all odd orders of side peaks split into triplets. The interval between the splitting increases monotonically with Φ, until it reaches the maximal value at $\Phi=\pi/2$, and then decrease monotonically down to zero at $\Phi=\pi$. Both triplet and doublet are asymmetric with respect to their splitting centers. It should also be noted that, for the triplet splitting in the incoherent fluorescence spectrum, the central component is always much stronger than the two side components. Another apparent consequence accompanied with these splittings is the dramatic deterioration in terms of line narrowing. Similar line splitting is observed in the absorption spectrum, as shown in Fig. 3(b). All even orders of side peaks split into the doublets and all odd orders of side peaks split into the triplets, with the maximal splitting taking place at $\Phi=\pi/2$. Similar to the incoherent fluorescence spectrum, the splittings are asymmetric about the splitting centers. On the other hand, there is a clear difference between the fluorescence and absorption spectra. In the latter, the central component of each triplet splitting is always much weaker

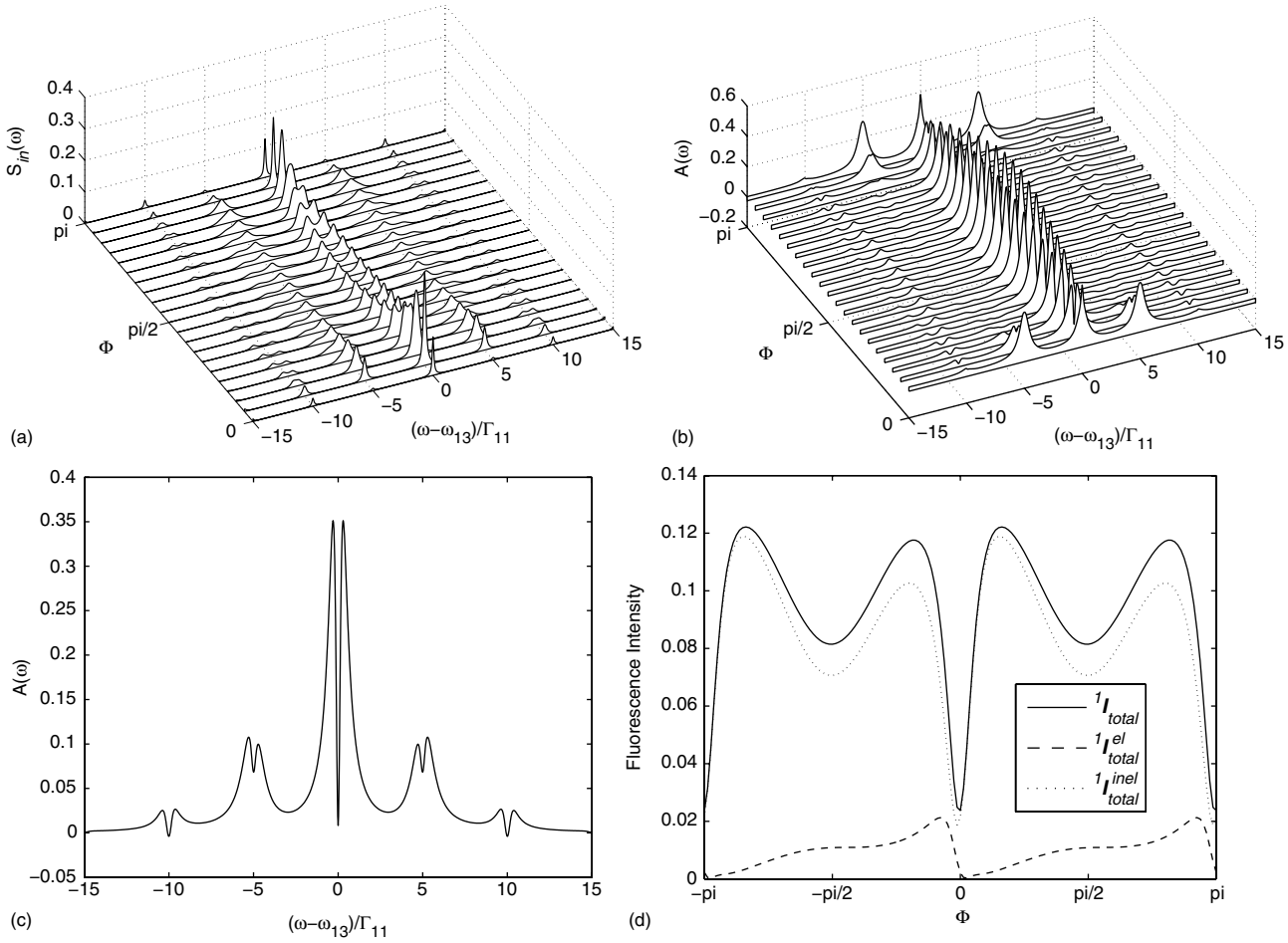

FIG. 3. (a) Incoherent fluorescence spectrum corresponding to the 1–3 transition, for several different values of Φ, with $\delta=5$, $\Delta_1=\Delta_2=0$, $\Omega_1=1$, and $\Omega_2=3$. Note the line splittings in all spectral lines. (b) Probe absorption spectrum corresponding to the 1–3 transition, for several different values of Φ. All parameters are the same with those for graph (a). Note the absorption dip on the central absorption peak. (c) Probe absorption spectrum corresponding to the 1–3 transition, with $\delta=5$, $\Phi=\pi/15$, $\Delta_1=\Delta_2=0$, $\Omega_1=1$, and $\Omega_2=3$. The FWHM of the central absorption dip is about $0.22\Gamma_{11}$. (d) Total fluorescence intensity corresponding to the 1–3 transition, plotted as a function of Φ, with $\delta=5$, $\Delta_1=\Delta_2=0$, $\Omega_1=1$, and $\Omega_2=3$. Solid, dashed, and dotted lines represent the total, elastic, and inelastic fluorescence intensities, respectively.

than the two side components, especially when Φ is small, the central component is so weak that the triplet apparently looks like a doublet. For clarity, we plot in Fig. 3(c) a probe absorption spectrum for $\Phi=\pi/15$. It is impressive that, although the splitting of each side peak is much smaller than the natural width, Γ_{11}, the sharp dips superimposed on top of the absorption peaks clearly exhibit the subnatural line splitting. The central absorption dip is so deep that it may even become a negative value implying amplification. We have numerically found that, if Φ is sufficiently small, the width of the dip at the central peak approaches $\frac{3}{2}\Gamma_{22}$ when $\Omega_2 \gg \Omega_1$. Further calculations (not shown here) show that, if the coupling field L_a is detuned, i.e., $\Delta_1 \equiv \omega_{13}-\omega_a \neq 0$, the absorption dips are also detuned from their resonant positions with the same amount of detuning, Δ_1. Now, Fig. 3(d) shows the total fluorescence intensity as a function of Φ, which also shows a modulation with a period of π. The global minimum of the total intensity occurs at $\Phi=0$. Within the full range of Φ, the inelastic fluorescence component makes a dominant contribution to the total intensity. The spectral dependence on the relative phase delay Φ provides an additional freedom in controlling the spectral features of the driven atom. We would like to point out that this phase-sensitive spectral behavior is a desirable result, since Φ is an experimentally controllable parameter, while the *absolute phase* of each field is very difficult to manipulate. It should be noted that, although the absolute phase of each laser field may experience random fluctuation, this fluctuation does not necessarily smear out the detailed spectral structure, provided that the effective laser bandwidth is well-controlled below the natural width of each atomic transition.

C. Effects of the Doppler broadening

Now we consider the effects of the Doppler-broadening in terms of the profiles of the absorption spectra. It is well known that the inhomogeneous Doppler-broadening in an atomic vapor can be experimentally eliminated by employing a counterpropagating probe beam. In the ordinary saturation spectroscopy with two-level atoms, if the coupling field is

detuned from the atomic transition frequency by v, the absorption of the counterpropagating probe field will exhibit a burning hole at detuning $-v$. This is attributed to the saturation of the group of atoms in which the Doppler-shift compensates the detuning of the coupling field. We find that, if the counterpropagating probe beam is sent into an atomic vapor and the phase delay, Φ, is maintained nonzero to introduce "saturation" on the atomic absorption peaks corresponding to the 1–3 transition, similar burning holes in the probe absorption also exist within our model, but now with a *subnatural* width.

We now assume that both coupling fields $L_{a,b}$, and the probe field are all in the collinear geometry, with both coupling fields propagating to the same direction while the probe field is propagating to the opposite direction. Figure 4 shows a representative absorption spectrum of the probe for the phase delay of $\Phi=\pi/15$. In the calculation the full width at the half maximum (FWHM) of the Doppler width D_1, for the 1–3 transition is chosen as $D_1=5$, and correspondingly the Doppler width of the 2–3 transition, D_2, is proportional to D_1 with the ratio of ω_{23}/ω_{13}. In this specific example, we assume that ω_{23}/ω_{13} is equal to $\frac{1}{2}$. As shown in Fig. 4(a), under the resonant condition, $\Delta_1=\Delta_2=0$, we find that the probe absorption spectrum spreads over a broad frequency range with an effective FWHM of about $5\Gamma_{11}$. Note the multiple narrow absorption dips in the spectrum. The central subnatural burning hole resides at exactly the atomic transition frequency ω_{13} with a FWHM of $0.25\Gamma_{11}$, while the side-dips at multiples of the modulation frequency show the less pronounced narrowing effect. For comparison, we present Fig. 4(b) for the case in which one of the coupling fields, L_a, is blue detuned, i.e., $\Delta_1\equiv\omega_{13}-\omega_a=-1$ and $\Delta_2=0$. It is clear that all the absorption dips are also blue detuned with the same amount of detuning as L_a. This shift of the absorption dips can be understood in terms of the shift of the absorption dips of the *stationary atoms*, which is, in principle, different from the burning holes induced by the *moving atoms* in the ordinary saturation spectroscopy. Further calculations (not shown here) show that the ratio ω_{23}/ω_{13} and the magnitude of Doppler width D_1 does not qualitatively affect the position and subnatural nature of the absorption dips, which allows us to make a general statement based on our arbitrary, but particular choice, of the parameters in Fig. 4.

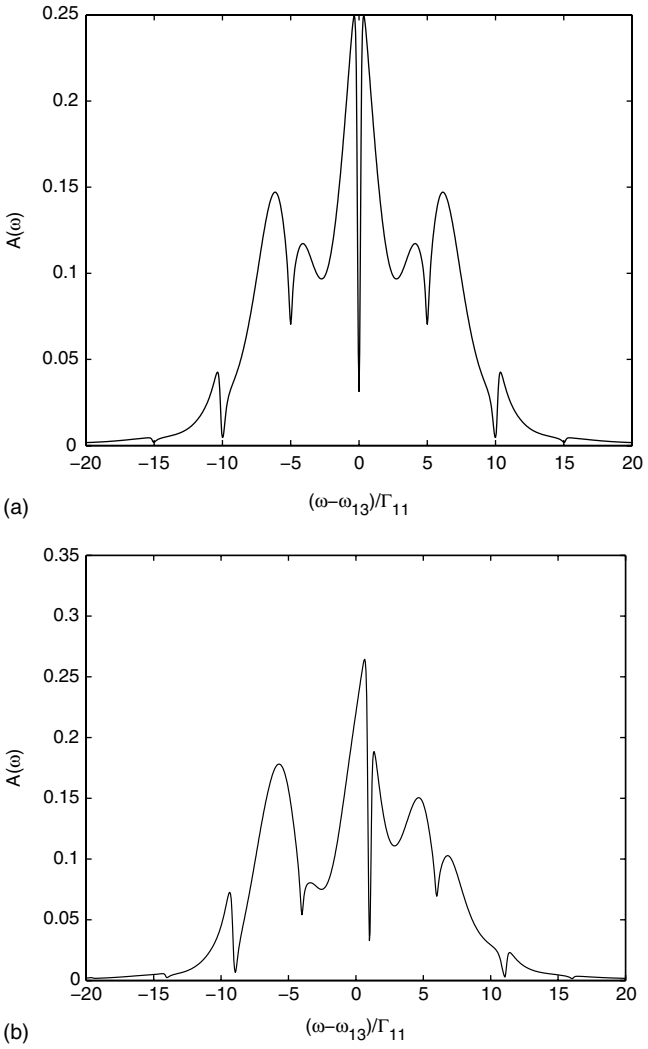

FIG. 4. (a) Probe absorption spectrum corresponding to the 1–3 transition for the counterpropagating probe beam geometry in an atomic vapor with a Doppler-broadening taken into account. Both bichromatic fields are on resonance ($\Delta_1=\Delta_2=0$), with $\Omega_1=1$, $\Omega_2=3$, $D_1=2D_2=5$, and $\Phi=\pi/15$. The FWHM of the central "burning hole" is about $0.25\Gamma_{11}$. (b) Same as (a) except that the bichromatic field L_a is blue detuned ($\Delta_1=-1$). Note the central burning hole is shifted to the blue side.

IV. CONCLUSION

In this paper we have theoretically studied the spectral properties of a *V*-type three-level atom driven by two bichromatic fields with a common frequency difference. Since Narducci *et al.* have studied the same system under two monochromatic fields [3], our work is a kind of extension of theirs. Therefore, the questions we have addressed at the beginning of this work is whether and how much *difference* as well as *similarity* we can see in the fluorescence and probe absorption spectra through the replacement of two monochromatic fields by two bichromatic fields. We have found that, although the fluorescence spectrum turns out to exhibit multipeak structure, it perfectly inherits the line-narrowing effect which has been found for the monochromatic fields. Moreover, we have found that the use of the bichromatic fields instead of the monochromatic fields provide a new doorknob to manipulate the spectral property through the experimentally controllable phase delay between the two bichromatic fields. Indeed, we have seen the significant phase sensitivities in terms of spectral line splittings, which lead to absorption dips with subnatural linewidths. A practical importance of this finding is that the subnatural linewidth can be observed as subnatural burning holes in an atomic vapor experiment.

ACKNOWLEDGMENTS

P.L. acknowledges the hospitality and the financial support at Kyoto University where this work has been initiated.

P.L. is also grateful to Dr. Chengpu Liu at Kyoto University for enlightening discussions and Dr. Beike Jia at University of Nevada for all the thoughtful conversations during the formation of this work. Part of the work by P.L. and the work by T.N. was supported by a Grant-in-Aid for scientific research from the Ministry of Education and Science of Japan. This work was also supported by National Science Foundation of China, Grant No. 10574030.

[1] B. R. Mollow, Phys. Rev. **188**, 1969 (1969); Phys. Rev. A **5**, 2217 (1972).
[2] H. Freedhoff and Z. Chen, Phys. Rev. A **41**, 6013 (1990); G. S. Agarwal, J. Opt. Soc. Am. B **8**, 1163 (1991); Z. Ficek and H. S. Freedhoff, Phys. Rev. A **48**, 3092 (1993); Z. Ficek, Prog. Opt. **35**, 389 (2000); Y. F. Zhu, Q. L. Wu, A. Lezama, D. J. Gauthier, and T. W. Mossberg, Phys. Rev. A **41**, 6574 (1990).
[3] L. M. Narducci, M. O. Scully, G.-L. Oppo, P. Ru, and J. R. Tredicce, Phys. Rev. A **42**, 1630 (1990); A. S. Manka, H. M. Doss, L. M. Narducci, P. Ru, and G.-L. Oppo, *ibid.* **43**, 3748 (1990); Cohen-Tannoudji, Jacques Dupont-Roc, and Gilbert Grynberg, *Atom-Photon Interactions* (Wiley, New York, 1992); D. J. Gauthier, Y. Zhu, and T. W. Mossberg, Phys. Rev. Lett. **66**, 2460 (1991).
[4] S. Papademetrious, S. Chakmakjian, and C. R. Stroud, Jr., J. Opt. Soc. Am. B **9**, 1182 (1992).
[5] M. F. Van Leeuwen, S. Papademetriou, and C. R. Stroud, Jr., Phys. Rev. A **53**, 990 (1996); S. Papademetriou, M. F. Van Leeuwen, and C. R. Stroud, Jr., *ibid.* **53**, 997 (1996); D. L. Aronstein, R. S. Bennink, R. W. Boyd, and C. R. Stroud, Jr., *ibid.* **65**, 067401 (2002).
[6] U. D. Rapol, A. Wasan, and V. Natarajan, Phys. Rev. A **67**, 053802 (2003).
[7] C. Goren, A. D. Wilson-Gordon, M. Rosenbluh, and H. Friedmann, Phys. Rev. A **69**, 063802 (2004).
[8] M. Jakob and G. Y. Kryuchkyan, Phys. Rev. A **57**, 1355 (1998).
[9] H. Wallis, Phys. Rev. A **52**, 1441 (1995).
[10] R. G. Unanyan, S. Guérin, and H. R. Jauslin, Phys. Rev. A **62**, 043407 (2000).